Eur. Phys. J. A **15**, 145–150 (2002)
DOI 10.1140/epja/i2001-10243-7

THE EUROPEAN PHYSICAL JOURNAL A

Large-scale shell model calculations for exotic nuclei

E. Caurier[1], F. Nowacki[1], and A. Poves[2,a]

[1] Institut de Recherches Subatomiques, IN2P3-CNRS-Université Louis Pasteur, F-67037 Strasbourg Cedex 2, France
[2] Departamento de Física Teórica, Universidad Autónoma de Madrid, Cantoblanco, 28049 Madrid, Spain

Received: 21 March 2002 /
Published online: 31 October 2002 – © Società Italiana di Fisica / Springer-Verlag 2002

Abstract. Recent shell model calculations for the neutron-rich nuclei around the magic numbers $N = 20$, $N = 28$ and $N = 40$ are reviewed. We stress two points: i) The crucial role played by the monopole part of the effective interaction that determines the evolution of the spherical mean field. In particular, the reduction in the quasiparticle gaps at the magic numbers can erode or even erase the shell closures. ii) The rich variety of structures that can be found in these situations, with coexisting deformed and spherical states, rapid changes of behaviour with N or Z, and the massive occurrence of intruder states as ground states.

PACS. 21.60.Cs Shell model – 21.60.-n Nuclear-structure models and methods – 21.10.Hw Spin, parity, and isobaric spin – 21.10.Ky Electromagnetic moments

1 Introduction

Large-scale shell model calculations give at present the most accurate and comprehensive description of light and medium light nuclei, including those at the very neutron-rich or very proton-rich edges. The success of this approach depends on two key aspects; the first is the use of large valence spaces that contain the most relevant degrees of freedom of the problem. The new shell model codes like ANTOINE and NATHAN from the Strasbourg group [1] and the new approximate methods of solving the nuclear secular problem such as the quantum Monte Carlo diagonalization method put forward by the Tokyo group [2] have been instrumental for this goal. The second is the improvement in our mastering of the effective "in-medium" nuclear interaction to be used in large valence spaces. This comes mainly from the work of A. Zuker and collaborators [3], who have shown that the multipole part of the interaction —responsible for the mixing and the correlations (pairing, quadrupole etc.)— is nearly universal. Besides, the effective interactions obtained from G-matrices, produce it correctly. At the same time, their theses on the role of the monopole part of the interaction (*i.e.* those terms that contribute to the spherical mean field, or in other words those that contain only number or isospin operators, either one or two body) have become commonly accepted. The monopole gives the skeleton upon which the coherent multipole terms build the structure of the nucleus. Other recent shell model studies of exotic nuclei include the Caltech Oak Rigde shell model Monte Carlo calculations of ref. [4] using effective interactions from the Oslo group [5] and the work of the MSU group [6]. The no-core shell model calculations of the Arizona group are also aiming to the description of very ligth exotic nuclei [7].

2 The N = 20 region

The region around ^{31}Na provides one of the best examples of intruder dominance in the ground states. This has been known experimentally [8–10] since long. Besides, early mean-field and shell model interpretations were also available that pointed out the role of deformed intruder configurations and delineated the so-called "island of inversion" [11–15]. Recently there has been a renewal of interest in this region, triggered by the advent of new radiactive ion beam facilities that pave the way towards spectroscopic studies far from stability. As a single example, let us quote the measure of the $B(E2)\uparrow$ of the ground state of ^{32}Mg by Coulomb excitation, that confirms its large deformation [16].

It serves also to illustrate the discussion on the role of the effective single-particle energies (ESPEs) in the predictions of a shell model calculation. In ref. [17] we had defined a model space (the full *sd*-shell for the valence protons and the full *pf*-shell for the valence neutrons) aimed to study the very neutron-rich isotopes with $Z < 20$. In the built up of the effective interaction, a number of reference nuclei were used to fix the evolution of the ESPE; ^{39,40,41}Ca, ^{47,48,49}Ca and the hole states

[a] e-mail: alfredo.poves@uam.es

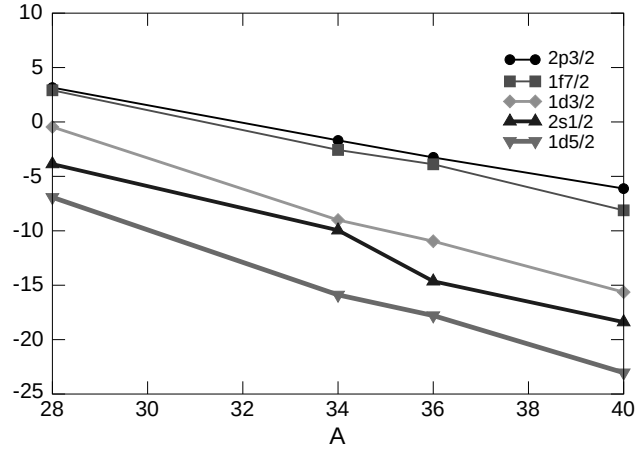

Fig. 1. Effective single-particle energies at $N = 20$ with the *sdpf*.sm interaction (in MeV).

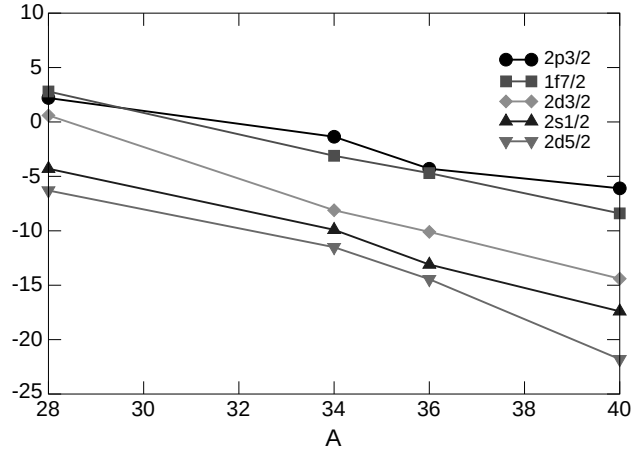

Fig. 2. Effective single-particle energies at $N = 20$ with the Tokyo group interaction (in MeV).

of the potassium isotopes. However, a key information was missing, the single-particle structure of ^{35}Si. A latter measurement [18] showed that the splitting $1f_{7/2}$-$2p_{3/2}$ was 1 MeV smaller than our prediction, and we modified the interaction accordingly.

In fig. 1 we have plotted the ESPEs at $N = 20$ for the four subshell closures $Z = 8, 14, 16$ and 20 using this interaction that we call *sdpf*.sm. Let us focus on their most important features:

i) The gap $1f_{7/2}$-$2p_{3/2}$ (fp) is steadily reduced from its initial value of 2 MeV at $Z = 20$ until almost zero at $Z = 8$.

ii) The gap $1d_{3/2}$-$1f_{7/2}$ (df) also diminishes from $\sim$ 7 MeV in ^{40}Ca to ~ 3 MeV in ^{28}O.

A 2p-2h neutron excitation across the closed $N = 20$ shell cost twice the value of the gap, therefore, the smaller it is the gap, the easier it is to break the shell closure. On the other side, the 2p-2h configurations may gain a lot of correlation energy due to the pairing interaction among like particles and to the quadrupole among protons and neutrons. In this last case a reduced fp gap enhances greatly the quadrupole coherence. It is well known that this mechanism is actually realized in nature giving rise to the so-called "island of inversion", an ensemble of nuclei around ^{31}Na whose ground states are dominated by intruder np-nh configurations. Notice that the precise definition of the limits of this region, as well as the actual amount of mixing between the coexisting states, depends critically on the values of the two gaps discussed above. To elaborate more on this point, we present in fig. 2 the ESPEs of the interaction used by the Tokyo group [19].

Both sets are equivalent between $Z = 20$ and $Z = 14$. From there on, they diverge; at $Z = 8$ the latter interaction produces a negative pf gap and halves the df gap of the *sdpf*.sm interaction. This is mainly due to the upwards shift of the $1d3/2$ orbit, resulting in an increased $N = 16$ neutron gap. Evidently this interaction will produce an enlarged island of inversion and enhanced correlations. Experiments will decide which choice is closer to reality. ^{24}O provides an excellent test case because the

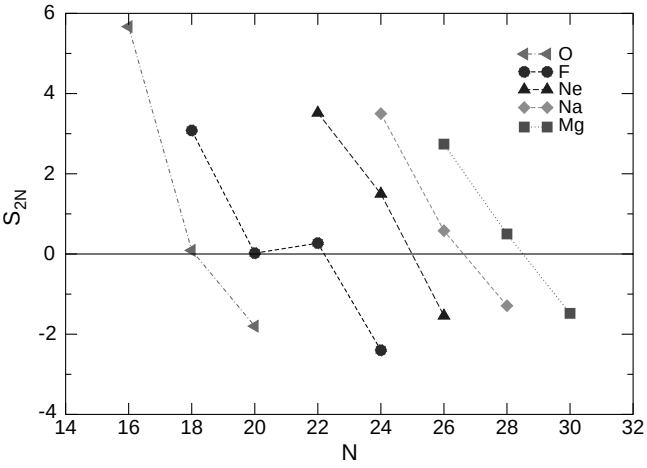

Fig. 3. Two-neutron separation energies (in MeV).

sdpf.sm interaction (which for its *sd* part is just USD) predicts the 2^+ at 4.4 MeV while the other places it close to 6 MeV. The spectrum of ^{25}F can also help in establishing the actual value of the $N = 16$ neutron gap.

It is important to stress that in the *sdpf* valence space, the structure of the oxygen isotopes is fully determined by the initial single-particle energies, that are taken from the experimental level scheme of ^{17}O, and by the $T = 1$ part of the effective interaction. Therefore, any modification of the shell structure already present in ^{17}O, that could occur in the heavier oxygen isotopes, must be caused enterely by the $T = 1$ channel of the effective interaction. Only when protons are added, the $T = 0$ channel, much more attractive, comes into play. The combined effect of both produces the known shell structure at the stability valley. The $T = 0$ channel does not have any influence in the evolution of the effective single-particle energies when only neutrons are present in the valence space.

The results for the $N = 20$ region using the interaction *sdpf*.sm have been recently gathered in [20]. We shall only discuss briefly the S_{2N} values of fig. 3. The neutron drip line is known for oxygen and fluorine, the last bound iso-

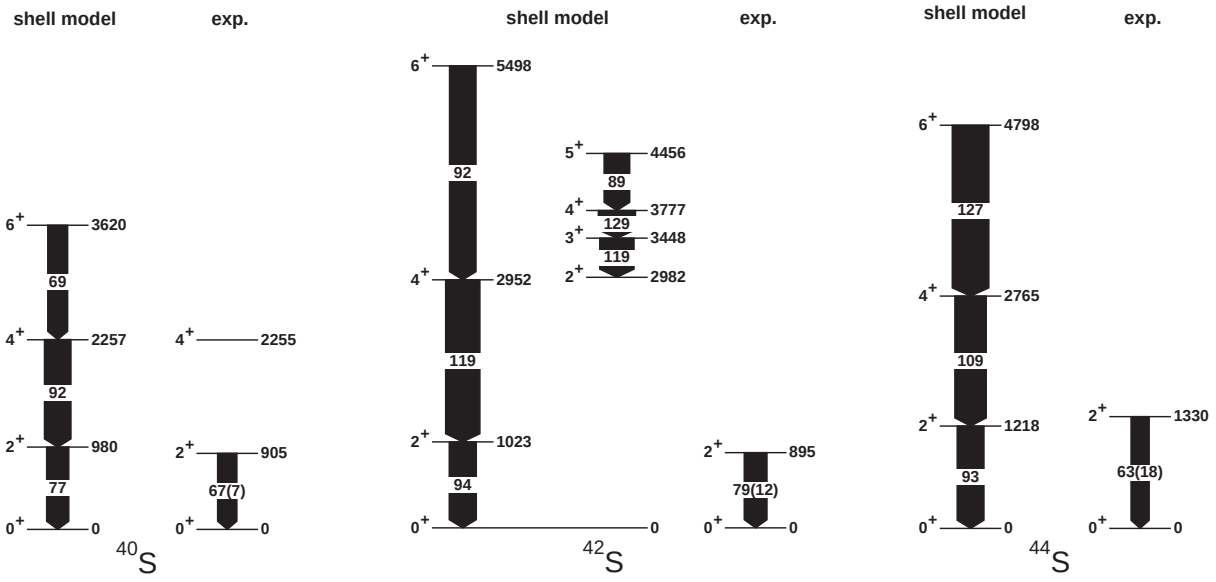

Fig. 4. Predicted level schemes of the heavy sulphur isotopes, compared with the experiment. Energies in keV, $B(E2)$'s in e^2 fm^4.

topes being ^{24}O and ^{31}F. The calculation gives $S_{2N} \sim 0$ for ^{26}O, ^{29}F and ^{31}F, compatible with the experiment. For the other chains, the situation is better defined, the predicted last bound isotopes being ^{34}Ne, ^{37}Na and ^{40}Mg.

Another striking manifestation of the intruder presence in the region has been recently found at Isolde [21]. The decay of ^{33}Na has shown that the ground state of ^{33}Mg has $J^\pi = 3/2^+$ instead of the expected $J^\pi = 3/2^-$ or $J^\pi = 7/2^-$. This inversion is nicely reproduced by our calculation.

Table 1.

	^{40}Mg	^{42}Si	^{44}S	^{46}Ar
$E^*(2^+)$ (MeV)	0.81	1.49	1.22	1.51
$E^*(4^+)$	2.17	2.68	2.25	3.46
$E^*(0_2^+)$	1.83	1.57	1.26	2.93
$Q(2^+)$ (e fm^2)	−21	16	−17	20
$BE2$ (e^2 fm^4)	108	71	93	93
$\left\langle n_{\frac{7}{2}} \right\rangle$	5.54	6.16	6.16	6.91
$\left(f_{\frac{7}{2}}\right)^8$ %	3	28	24	45

3 The N = 28 region

With the same interaction, we have studied the neutron-rich isotopes of Mg, Si, S and Ar. As we remove protons from ^{48}Ca, the fp gap diminishes and therefore the closed-shell configuration becomes vulnerable. This would be the case if it is energetically more convenient to promote neutrons across the gap, recovering the cost in single-particle energies by the gain in neutron proton quadrupole correlation energy. This effect is clearly seen in table 1, where we gather the results for the $N = 28$ isotones. ^{46}Ar has, to a good extent, a closed neutron shell, however in ^{44}S and ^{42}Si the ground state is a complicated mixture of closed shell and np-nh excitations. This mixing produces a very low-lying first excited 0^+ in both nuclei that might be taken as a signature of spherical-deformed coexistence at the mean-field level. In ^{40}Mg the 2p-2h components fully dominate.

In fig. 4 we have plotted the yrast bands of the heaviest known sulphur isotopes. The agreement with the experimental results [22] is excellent and extends to the new data presented in this conference [23]. In our calculation ^{42}S behaves as a very regular prolate rotor, with an incipient excited γ band. The situation in ^{44}S is not easily cast in the language of the intrinsic frame. The low-energy level scheme of ^{43}S has been recently obtained at Ganil and MSU [24]. Surprisingly the first-excited state is isomeric. According to our results the ground state would be deformed and have spin $3/2^-$. The spherical single hole state $7/2^-$ is the first-excited state and his lifetime is consistent with that of the experimental isomer. The third known state is short lived and, according to the calculation, it may correspond to the $7/2^-$ member of the ground-state band.

Although most experimental data in the region are in agreement with the shell model description using the interaction *sdpf*.sm, more data on heavy silicons and magnesiums are needed in order to have a fully consistent picture.

4 The N = 40 region

The pf-shell is the present paradigm of the shell model description of atomic nuclei, as the sd-shell was in the '80s. However, the harmonic-oscillator shell closure at $N = Z = 80$ is known not to hold. ^{80}Zr is a well-deformed nucleus due to the merging of the $1g_{9/2}$ and $2d_{5/2}$ orbits with the

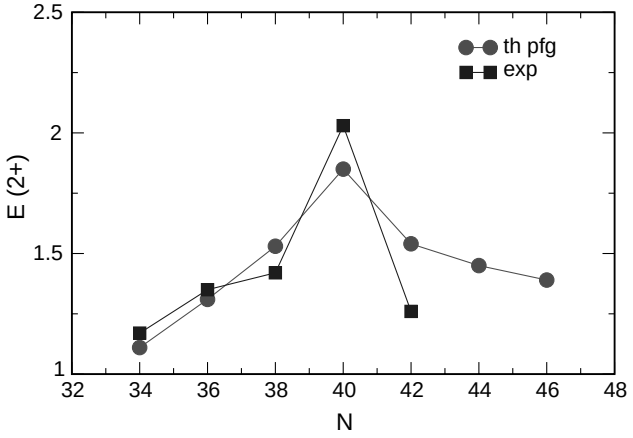

Fig. 5. Excitation energy of the 2^+ states in MeV: Ni isotopes.

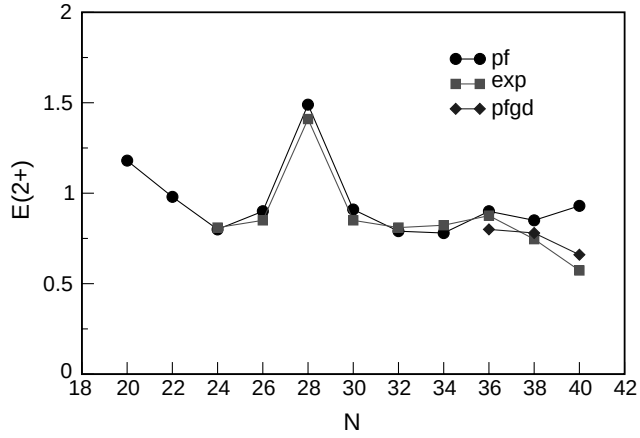

Fig. 7. Excitation energy of the 2^+ states in MeV: Fe isotopes.

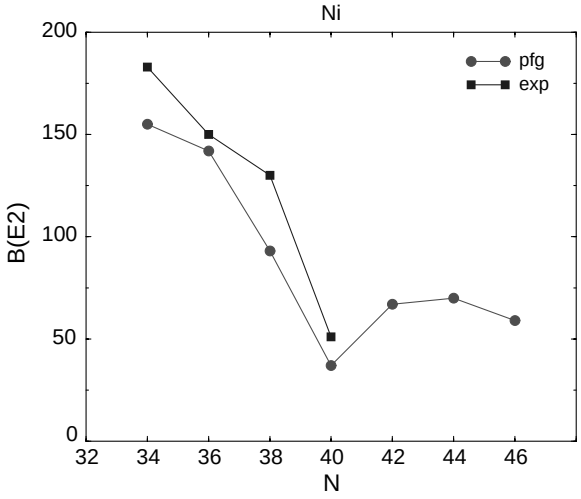

Fig. 6. $B(E2)$ $2^+ \rightarrow 0^+$ in e^2 fm^4: Ni isotopes.

upper pf-shell orbits. The situation at the neutron-rich side, the area around ^{68}Ni is less clear. The quasiparticle gap is not very large, $\sim$ 3 MeV, and one could expect strong scattering of pairs from the $2p_{1/2}$ and $1f_{5/2}$ orbits towards the $1g_{9/2}$. This is also indicated by the fact that the experimental S_{2N}'s of ^{68}Ni and ^{70}Ni are almost equal, thus not showing any shell closure effect. Therefore, in order to encompass these nuclei, the pf-shell valence space has to be enlarged to include at least the $1g_{9/2}$ orbit (it could be necessary to include the $2d_{5/2}$ too because of the role it plays in the built up of quadrupole coherence when protons and neutrons are active). We have worked in two different valence spaces that we refer to as pfg and $pfgd$. In pfg we take a closed ^{48}Ca core and allow for neutron excitations into the $1g_{9/2}$ orbit. In $pfgd$ we take a closed ^{52}Ca core but allow for neutron excitations into the $1g_{9/2}$ and $2d_{5/2}$ orbits. We have verified that for the Ni isotopes both spaces produce equivalent results. For the heavy Cr's and Fe's, the use of the space $pfgd$ turns out to be necessary to take into account fully the quadrupole coherence. The effective interaction is based in the G-matrix of ref. [25] with the modifications of ref. [26]. The matrix elements involving the $2d_{5/2}$ orbits are taken from the Kahana, Lee and Scott G-matrix [27].

The low-energy spectrum of ^{68}Ni is very well reproduced by the calculation; the excited 0^+ at 1.85 MeV, 2^+ at 2.15 MeV, 5^- at 2.72 MeV and 4^+ at 3.10 MeV fit remarkably well the experimental results. The ground-state wave function is 40% closed shell, but a single 2p-2h state (corresponding to a $J = 0$ $T = 1$ pair jump from $1f_{5/2}$ to $1g_{9/2}$) appears also with a 25% probability . Small modifications of the pf-g gap favour one or another without altering drastically the rest of the properties. This gives to ^{68}Ni a hybrid status of superfluid and closed shell. The first excited 0^+ has a larger 2p-2h content which is more dispersed among several states.

In fig. 5 we compare the excitation energy of the 2^+ states in the Ni chain with the available experimental data (including the very recent ^{70}Ni value [28]. The agreement is fair, although the experiment gives a larger peak at $N = 40$. Similarly the $B(E2)$'s in fig. 6 follow the experimental trends including the recent ^{68}Ni measure [28]. The very sharp drop of the $B(E2)$ at $N = 40$ could be taken as an indication of a shell closure. However, if this were the case, this value must be much weaker. This is due to the fact that $N = 40$ is an harmonic-oscillator shell closure. Thus, the lowest 2^+ state is produced by a 2p-2h configuration and in this limit, the $B(E2)$ is strictly zero. Thus, all the transition probability is due to the breaking of the $N = 40$ magicity. In the $N = 20$ harmonic-oscillator doubly magic closure, ^{40}Ca, the $B(E2)$ is almost an order of magnitude smaller. Beyond $N = 40$ the calculations predict a modest increase of the $B(E2)$'s.

With this weak $N = 40$ closure, one should expect that, if the $1f_{7/2}$ proton shell were not completely filled, the system could be led into deformed solutions. We have examined this issue in the Cr and Fe chains using the space $pfgd$ for the heavier isotopes. We have also made a full pf-shell calculation using the interaction KB3G [29] for the isotopes from $N = 20$ to $N = 40$. The results for the 2^+ excitation energies are presented in figs. 7 and 8.

Notice that the pf-shell calculation gives an excellent description of the experimental data up to $N = 36$. Beyond, the drop in excitation energy, experimentally seen in

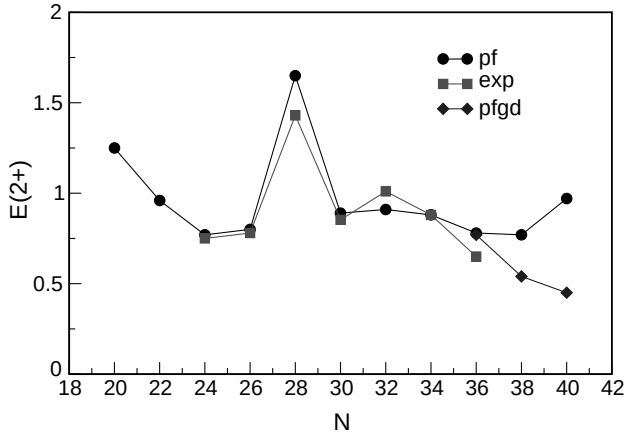

Fig. 8. Excitation energy of the 2^+ states in MeV: Cr isotopes.

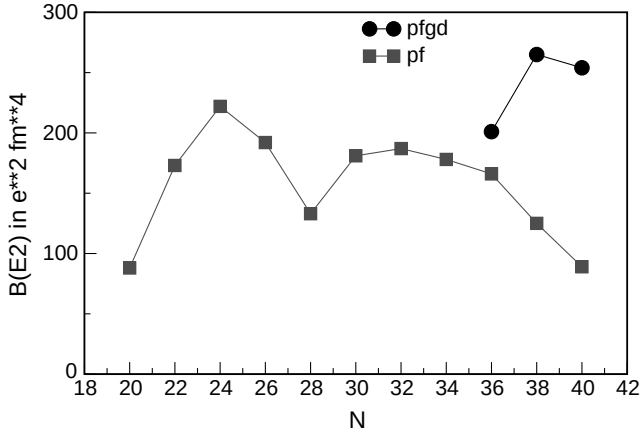

Fig. 10. $B(E2)$ $0^+ \rightarrow 2^+$ in e^2 fm^4: Cr isotopes.

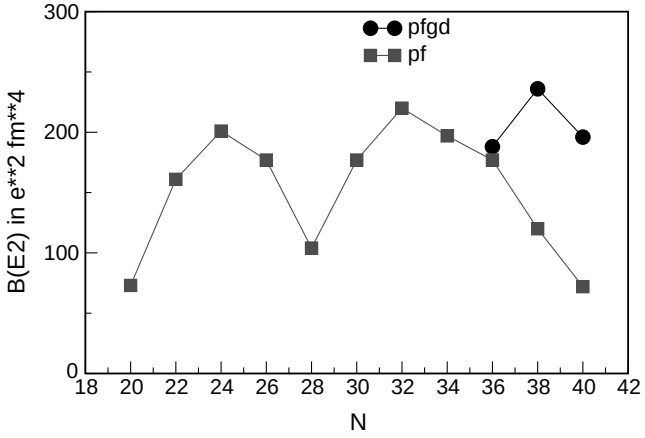

Fig. 9. $B(E2)$ $0^+ \rightarrow 2^+$ in e^2 fm^4: Fe isotopes.

the Fe isotopes [30] and in the Cr isotopes [31] requires the inclusion of the upper orbits. This is also the case for the $B(E2)$'s, as can be seen in figs. 9 and 10. For instance, in ^{66}Fe, the pf-shell prediction of 50 e^2 fm^4 rises to 200 e^2 fm^4 in the $pfgd$ space. The calculation also produces very low-lying 2^+'s in ^{62}Cr and ^{64}Cr, consistent with large $B(E2)$ values ($\sim$ 250 e^2 fm^4) corresponding to $\beta = 0.27$. Hence, we predict the existence of a new region of deformation at $N = 40$.

5 Conclusions

We have seen how the modification of the single-particle structure as the neutron excess is increased may lead to the appearance of new physical phenomena. In the first place we have examined the island of inversion around ^{31}Na, explaining its occurrence as due to two combined effects; the reduction of the *sd-pf* gap as the nuclei get more neutron rich and the large correlation energy of the 2p-2h configurations in the nuclei with half-filled $1d_{5/2}$ proton orbit.

The erosion or vanishing of the $N = 28$ closure is somehow different, because the excited orbits have the same parity than the closed $1f_{7/2}$. In ^{40}Mg, we predict a complet disappearance of the $N = 28$ magicity, while in ^{42}Si and ^{44}S the closed shell and the excited configurations are fully mixed. We find also the presence of coexisting shapes, sometimes producing isomeric states.

At $N = 40$, the pf-sdg gap is easily ovecome by the pairing interaction that scatters $J = 0$ $T = 1$ pairs from the pf-shell into the $1g_{9/2}$ orbit. This explains the strange behaviour of ^{68}Ni. In the nuclei where the $1f_{7/2}$ proton shell is not filled, the neutrons excited to the *sdg*-shell couple to the pf-protons and deformation appears. The removal of two or four protons from the spherical ^{68}Ni, drives ^{66}Fe and ^{66}Cr into prolate shapes generating a new region of deformation.

This work is supported by the Spanish Ministry of Science and Technology under grant BFM2000-30 and by the IN2P3 (France)-CICyT (Spain) collaboration.

References

1. E. Caurier *et al.*, Phys. Rev. C **59**, 2033 (1999).
2. M. Honma, T. Mizusaki, T. Otsuka, Phys. Rev. Lett. **77**, 3315 (1996).
3. M. Dufour, A.P. Zuker, Phys. Rev. C **54**, 1641 (1996).
4. D.J. Dean *et al.*, Phys. Rev. C **59**, 2474 (1999).
5. M. Hjort-Jensen, T.T. Kuo, E. Osnes, Phys. Rep. **261**, 125 (1995).
6. A. Navin *et al.*, Phys. Rev. Lett. **85**, 266 (2000).
7. P. Navratil, J.P. Vary, B.R. Barret, Phys. Rev. Lett. **84**, 5728 (2000).
8. C. Thibault *et al.*, Phys. Rev. C **12**, 193 (1975).
9. D. Guillemaud *et al.*, Nucl. Phys. A **246**, 37 (1984).
10. G. Klotz *et al.*, Phys. Rev. C **47**, 2502 (1993).
11. X. Campi, H. Flocard, A.K. Kerman, S. Koonin, Nucl. Phys. A **251**, 193 (1975).
12. A. Poves, J. Retamosa, Phys. Lett B **184**, 311 (1987); Nucl. Phys. A **571**, 221 (1994).
13. E.K. Warburton, J.A. Becker, B.A. Brown, Phys. Rev. C **41**, 1147 (1990).

14. N. Fukunishi, T. Otsuka, T. Sebe, Phys. Lett. B **296**, 279 (1992); T. Otsuka, N. Fukunishi, Phys. Rep. **264**, 297 (1996).
15. K. Heyde, J.L. Woods, J. Phys. G **17**, 135 (1991).
16. T. Motobayashi *et al.*, Phys. Lett. B **346**, 9 (1995).
17. J. Retamosa, E. Caurier, F. Nowacki, A. Poves, Phys. Rev. C **55**, 1266 (1997).
18. S. Nummela *et al.*, Phys. Rev. C **63**, 044316 (2001).
19. Y. Utsuno, T. Otsuka, T. Mizusaki, M. Honma, Phys. Rev. C **60**, 054315 (1999).
20. E. Caurier, F. Nowacki, A. Poves, Nucl. Phys. A **693**, 374 (2001).
21. S. Nummela *et al.*, Phys. Rev. C **64**, 054313 (2001).
22. T. Glasmacher, Annu. Rev. Nucl. Part. Sci. **48**, 1 (1998).
23. F. Azaiez *et al.*, this issue, p. 93.
24. F. Sarazin *et al.*, Phys. Rev. Lett. **84**, 5062 (2000); R.W. Ibbotson *et al.*, Phys. Rev. C **59**, 642 (1999).
25. J. Shurpin, T.T.S. Kuo, D. Strottman, Nucl. Phys. A **408**, 591 (1986)
26. F. Nowacki, PhD Thesis, Ires, Strasbourg 1996.
27. S. Kahana, H.C. Lee, K. Scott, Phys. Rev. **180**, 956 (1969).
28. F. Azaiez, in *ENPE99*, edited by B. Rubio, M. Lozano, W. Gelletly, AIP Conf. Proc. **495**, 171 (1999); O. Sorlin *et al.*, Phys. Rev. Lett. **88**, 092501 (2002).
29. A. Poves, J. Sánchez Solano, E. Caurier, F. Nowacki, Nucl. Phys. A **694**, 157 (2001).
30. M. Hannawald *et al.*, Phys. Rev. Lett. **82**, 1391 (1999).
31. O. Sorlin *et al.*, Nucl. Phys. A **669**, 351 (2000); **682**, 183c (2001).